RESEARCH ARTICLE | NOVEMBER 17 2023

## Ultrathin MXene film interaction with electromagnetic radiation in the microwave range **② ⊘**

Roman Rakhmanov ⊚ ; Christopher Eugene Shuck ⊚ ; Jamal Al Hourani ⊚ ; Stefano Ippolito ⊚ ; Yury Gogotsi ➡ ⊚ ; Gary Friedman ➡



Appl. Phys. Lett. 123, 204105 (2023) https://doi.org/10.1063/5.0176575









# Ultrathin MXene film interaction with electromagnetic radiation in the microwave range (1)

Cite as: Appl. Phys. Lett. **123**, 204105 (2023); doi: 10.1063/5.0176575 Submitted: 14 September 2023 · Accepted: 30 October 2023 · Published Online: 17 November 2023







Roman Rakhmanov,<sup>1,2</sup> (i) Christopher Eugene Shuck,<sup>2</sup> (i) Jamal Al Hourani,<sup>1,2</sup> (i) Stefano Ippolito,<sup>2</sup> (i) Yury Gogotsi,<sup>2,a)</sup> (ii) and Gary Friedman<sup>1,a)</sup>

## **AFFILIATIONS**

<sup>1</sup>Department of Electrical and Computer Engineering, Drexel University, 3141 Chestnut St, Philadelphia, Pennsylvania 19104, USA <sup>2</sup>A. J. Drexel Nanomaterials Institute, Department of Materials Science and Engineering, Drexel University, 3141 Chestnut St, Philadelphia, Pennsylvania 19104, USA

<sup>a)</sup>Authors to whom correspondence should be addressed: yg36@drexel.edu and gf29@drexel.edu

## **ABSTRACT**

The quick progress in communication technologies demands superior electromagnetic interference (EMI) shielding materials. However, achieving a high shielding effectiveness (SE) with thin films, which is needed for microscale, flexible, and wearable devices, through absorption of EM radiation remains a challenge. 2D titanium carbide MXene,  $Ti_3C_2T_x$ , has been shown to efficiently reflect electromagnetic waves. In this paper, we investigated the electromagnetic shielding of ultrathin printed  $Ti_3C_2T_x$  films and recorded absorption up to 50% for 4 nm-thick films. This behavior is explained by impedance matching. Analysis of the sheet impedance in the X-band frequency range allows us to correlate the EMI shielding mechanism with the electrical conductivity measured within the same range. The average bulk in-plane conductivity for 4 to 40 nm-thick films reaches  $10^6$  S/m, while the average relaxation time is estimated at around 2.3 ps. Our figures of merit are similar to those reported for ultrathin metal films, such as gold, showing that an abundant MXene material can replace noble metals. We demonstrate that the MXene conductivity mechanism does not change from direct current to THz. The conventional method of reporting EMI SE is correlated with absolute values of transmitted, reflected, and absorbed power, which allows us to interpret previous results on MXene EMI shielding. Considering the easy deposition of thin MXenes films from solution onto a variety of surfaces, our findings offer an attractive alternative for shielding microscale devices and personal electronics.

Published under an exclusive license by AIP Publishing. https://doi.org/10.1063/5.0176575

The expansion of communication networks demands effective protection from destructive signal interference. <sup>1,2</sup> Conventional absorbers are heavy while absorbing metasurfaces, and heterostructures<sup>3</sup> are usually narrowband and require meticulous fabrication. Metals are highly reflective, which is not desired for shielding as it leads to electromagnetic pollution. However, ultrathin metallic films deposited on a substrate exhibit properties different from bulk metals. This is due to the film morphology affecting the electronic transport, allowing for the matching of the characteristic film impedance with that one of free space. This leads to higher absorption (up to 50%) of electromagnetic energy across a broad range of frequencies. <sup>4,5</sup> This phenomenon has been extensively studied on ultrathin metal film, specifically on gold (Au), as it allows for continuous film deposition. The impedance matching condition is reached for Au films possessing a thickness of a few nanometers and conductivity of 10<sup>6</sup> S/m, which is

40 times less than the value recorded for bulk Au, and it has been extensively studied in the THz range.  $^{6-10}$ 

MXenes are a class of 2D transition metal carbides, nitrides, and carbonitrides with the general formula of  $M_{n+1}X_n$ , where M is an early transition metal (Ti, V, Nb, ...), X is a C and/or N, and n is 1-4. <sup>11–13</sup> MXenes have received significant attention due to their singular and versatile properties, such as high metallic conductivity, exceeding  $2.0 \times 10^6$  S/m, tunable chemistry as well as strong hydrophilicity, promoting cost-effective MXene deposition on a broad variety of surfaces. <sup>14</sup> In particular,  $Ti_3C_2T_x$  is among the most studied and stable MXenes, showing extremely high conductivity. These properties have encouraged the extensive use of MXenes for Internet of Things (IoT) applications, such as electromagnetic interference (EMI) shielding <sup>15,16</sup> and microwave circuit components. MXene films with thicknesses below skin depth used for transmission lines and antennas have shown

performance comparable with metals.  $^{17-19}$  In these works, it has been demonstrated that  $\mathrm{Ti_3C_2T_x}$  exhibits high conductivity in both direct current (DC) and alternate current (AC) measurements. It is also possible to incorporate MXenes into composites to produce multifunctional materials with high EMI shielding performance. Moreover, MXenes-based devices show high performance up to the THz range.  $^{21-23}$  Electronic conductivity has been hypothesized to be the main contributor to such performances; however, there is an unexplained nonlinear drop recorded for submicrometer-thick films.

There are various methods to analyze the performance of thin conductive films in the microwave range. Resonant methods are accurate but narrowband,<sup>25</sup> and transmission-reflection line (TRL) methods<sup>26,27</sup> are limited by the transmission through the sample and require assumptions that can influence the accuracy of the method. The microwave impedance extraction done by Wang et al.<sup>28</sup> is a TRL method that uses waveguide discontinuity caused by the sample to increase the measurement accuracy. The method characterizes the gap between two waveguides formed by substrate insertion and the conductive film deposited on the substrate. This allows extraction of the film's sheet impedance, eliminating the substrate influence and increasing measurement accuracy. Accuracy is increased by measuring reflection from the backside of the sample, as losses due to waveguide discontinuity lower the reflection values. This avoids instabilities reported for other methods, allowing for the analysis of highly conductive materials.

In this paper, we elucidate the EMI shielding performance of  $Ti_3C_2T_x$  by measuring its sheet impedance in the X-band (8.2–12.4 GHz) frequency range and compare the obtained data with previous results. <sup>15,29</sup> We report high intrinsic absorbance for nm-thick  $Ti_3C_2T_x$  films due to the impedance matching with the free space medium. Waveguide measurements of sheet impedance were used to analyze the performance of the films. Sheet impedance was used to calculate the conductivity of the film based on measured thickness. Results are verified by the 4-point probe measurements in the DC range. The imaginary part of conductivity was used to estimate electron relaxation time based on the Drude model. This allows the interflake transport analysis via microwave measurements.

The interaction of thin conductive films with electromagnetic radiation can be described by the transmission line method. Propagation of the wave within a medium is described by the impedance, given by the ratio between tangential components of the electric and magnetic fields. To rothin conductive films with thickness d below skin depth, the transverse electric field induces current density that is equally distributed along the film. The impedance of such film can be expressed as 1

$$z = \frac{E}{I} \approx \frac{1}{\sigma d}.$$
 (1)

For a supported film, impedance can be represented as

$$Z_L = \frac{1}{Z} + \frac{\grave{1}}{Z_s},\tag{2}$$

where the substrate impedance  $Z_s$  can be neglected when the film thickness is much less than the wavelength. Reflection and transmission coefficients from the surface of the film can be expressed as

$$r = \frac{Z_L - Z_0}{Z_L + Z_0},\tag{3}$$

$$t = \frac{2Z_l}{Z_L + Z_0}. (4)$$

Here,  $Z_0$  is the free space impedance, which, for an empty waveguide, is expressed as  $Z_0 = \omega \mu_0 / \sqrt{\left(1 - \frac{\omega_c^2}{\omega^2}\right)}$ . Experimentally, reflection and transmission coefficients are measured in terms of Scattering parameters. Reflected and transmitted power can be expressed as  $R = |S_{11}|^2$ ,  $T = |S_{21}|^2$ . Absorbance is calculated as A = 1 - R - T and reaches the maximum when the film characteristic impedance equals half of free space impedance  $Z = Z_0/2$ .

The logarithmic scale is often used to represent shielding effectiveness (SE), and it is the main metric of performance. The following formulations allow for quantitative analysis of the total shielding effectiveness. Total shielding effectiveness  $SE_T$  considers a fraction of the transmitted energy,

$$SE_T = 10 \log_{10} \left(\frac{1}{T}\right). \tag{5}$$

Reflection effectiveness  $SE_R$  describes how much power is left after reflection,

$$SE_R = 10 \log_{10} \left( \frac{1}{1 - R} \right).$$
 (6)

Effective absorption  $SE_A$  is defined as the difference between these two values,

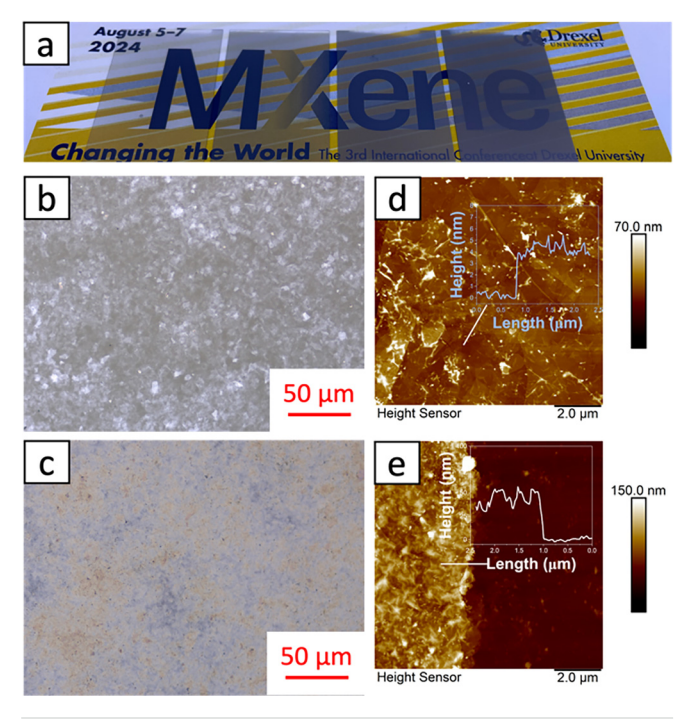


**FIG. 1.** (a) Picture of spray-coated films with different thicknesses (left to right: 4, 15, 25, and 40 nm), (b) optical image of a 4 nm-thick  $Ti_3C_2T_x$  film taken with an optical microscope, (c) optical image of a 40 nm-thick  $Ti_3C_2T_x$  film taken with an optical microscope, (d) AFM images of a 4 nm-thick and (e) 40 nm-thick  $Ti_3C_2T_x$  film.

$$SE_A = 10 \log_{10} \left( \frac{1 - R}{T} \right). \tag{7}$$

These formulations assume reflection dominated interaction with electromagnetic waves as  $SE_A$  and  $SE_T$  correspond to the power remaining after reflection. With increasing reflection and diminishing transmission, the calculated  $SE_A$  value becomes increasingly large. As reflection becomes dominant, absorbed and transmitted power decrease, leading to high  $SE_A$  values that do not correspond to the absorbed power. These factors can lead to confusion when reporting results  $^{33,34}$ 

Measurement of the film performance at microwave range requires accounting for the presence of the substrate. The method reported by Wang  $et~al.^{28}$  allows for the analysis of conductive films at microwave range and de-embed films performance from the substrate. This is achieved by representing the conductive film deposited on a substrate as a cascade network through ABCD parameters [Eq. (8)], which are easily recalculated into measured S-parameters. The first matrix represents thin  ${\rm Ti}_3C_2{\rm T}_x$  MXene film, where  $Y_f$  is the admittance of the film. The following two matrices represent the substrate as  $\Pi$ -circuit, which contains admittance and impedance of the gap introduced by substrate  $Y_g=1/Z_g$ ,

$$\begin{bmatrix} A_t & B_t \\ C_t & D_t \end{bmatrix} = \begin{bmatrix} 1 & 0 \\ Y_f & 1 \end{bmatrix} \begin{bmatrix} 1 & 0 \\ Y_g & 1 \end{bmatrix} \begin{bmatrix} 1 & Z_g \\ 0 & 1 \end{bmatrix} \begin{bmatrix} 1 & 0 \\ Y_g & 1 \end{bmatrix}.$$
(8)

Substrate parameters are measured independently and later used to evaluate the performance of the film through the calculated gap parameters. Energy leaks introduced by the gap decrease the reflection from the backside of the film, leading to better accuracy. Film impedance can be expressed by the following equation:

$$Z_f = \frac{1}{Y_f} = \frac{S_{21}Z_0}{1 - S_{22} - S_{21} - Z_0 Y_{gp} (1 + S_{22} + S_{21})}.$$
 (9)

MXene aqueous colloidal suspensions were prepared following previously reported methods.<sup>36</sup> Borosilicate glass with thickness of 150um was used as a substrate. The substrate thickness was chosen to fit microwave method requirements. A plasma cleaner was used to increase the substrate wettability, using an Ar/O2 gas mixture of 3/5 sccm at 100 W. MXene films [Fig. 1(a)] were deposited onto plasma-treated substrates by a spray-coating method. Film thicknesses were chosen to be semitransparent to allow for the applicability of the waveguide measurement, as it depends on both reflection (S<sub>11</sub>) and transmission (S<sub>21</sub>) coefficients. Optical images of the film surfaces [Figs. 2(b) and 2(c)] were taken using a Keyence optical microscope. Films show a rough surface, where roughness decreases with increasing thickness. Surface roughness and film thickness [Figs. 1(d) and 1(e)] were measured using atomic force microscopy (AFM). Films thicknesses were equal to 4, 15, 25, and 40 nm, while their corresponding surface roughness was 2, 8, 10, and 12 nm.

Microwave measurements were conducted using a Keysight PNX vector network analyzer (VNA). Transmission-reflection-line calibration (TRL) of the VNA was made with a Keysight WR90 calibration kit (8.2–12.4 GHz, X-band). The intermediate frequency (IF) bandwidth was set to 30 kHz, averaging 10 scans per measurement.

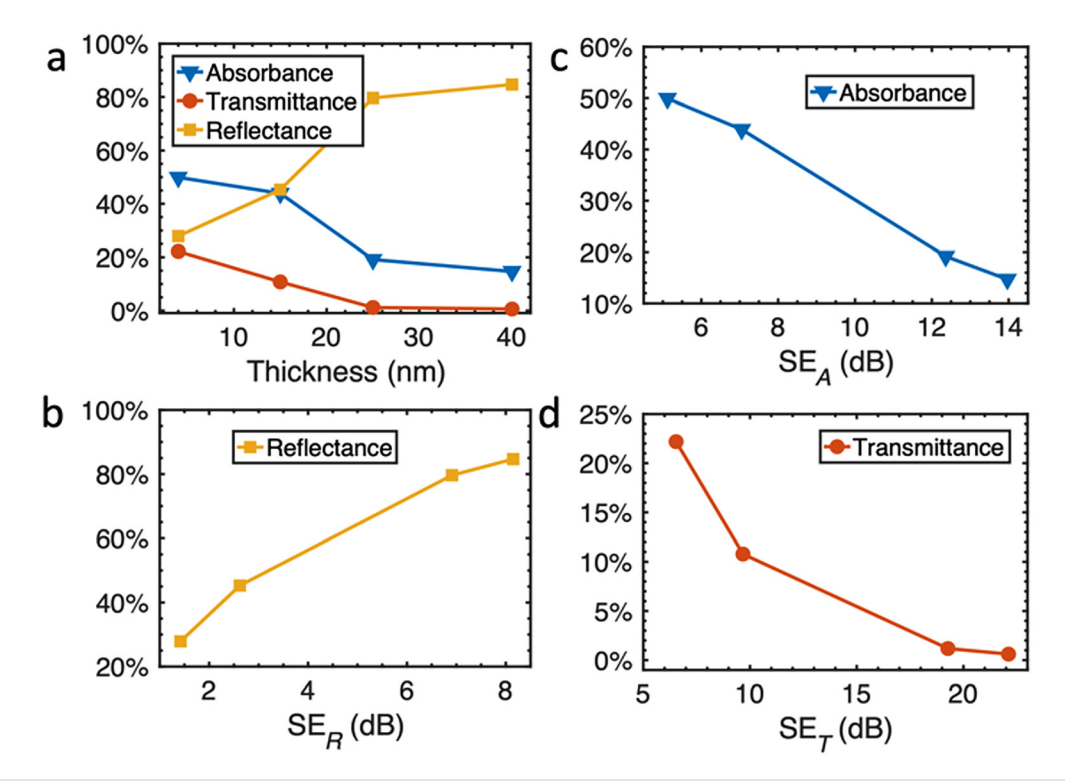


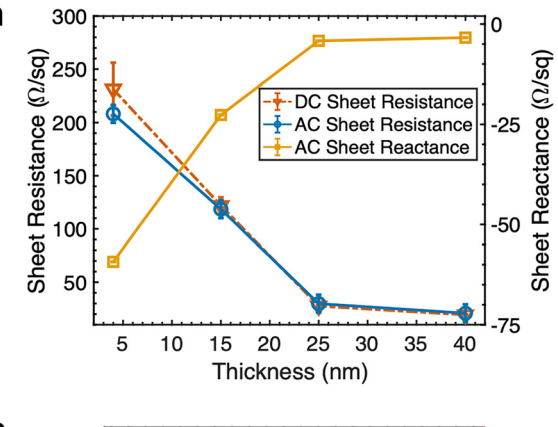
FIG. 2. (a) Change of reflection, transmission, and absorption with a thickness of spray-coated  $T_{13}C_2T_x$  films. At 8 nm, 50% absorption is observed. As the thickness is increased, the absorption decreases and reflection becomes dominant, correlation of (b) reflectance to  $SE_R$  (c) of absorbance to  $SE_R$  (d) transmittance to  $SE_T$ .

Samples were placed in between two halves of the waveguide. DC sheet resistance measurements are done by the Keithley 4-point probe.

The experimentally measured reflected, transmitted, and absorbed power is plotted as a function of thickness in Fig. 2(a). The behavior is independent of frequency, and, thus, the results are averaged across the measured frequency range, as reported in Figs. S1(a)-S1(c). At low thickness values, absorption is dominant, reaching 50% of total power for a 4 nm-thick film, while the reflection and transmission are both 25%. When the thickness increases up to 40 nm, reflection becomes dominant as it increases up to 80%. The absorption decreases to 20%, while transmission becomes negligible. In Figs. 2(b)-2(d), the results are plotted in terms of shielding effectiveness, commonly used to quantify shielding performance. All three shielding effectiveness parameters increase with thickness and appear uncorrelated to the change in reflected, transmitted, and absorbed power, due to the previously highlighted formulations of shielding effectiveness parameters Eqs. (5)–(7).  $SE_R$  determines the amount of power left after the reflection, and when the reflection increases, the ratio of power remaining after reflection to transmitted power increases, leading to higher values of SE<sub>A</sub> while the amount of absorbed power decreases.

Experimental results agree with previously reported results for spray-coated films as well as for monolayer assemblies. In the work by Han et~al.,  $^{15}$  Ti $_3$ C $_2$ T $_x$  film thickness ranged from 1 to 138 nm. At 11 nm, the SE $_A$  value is 7 dB, which is close to 50% absorption. Differences with this work might be due to synthesis protocols or errors in the determination of the thickness using the UV-Vis method. Variations can be also due to inconsistencies due to the spray-coating deposition method. Ti $_2$ C films analyzed in the same work with 25 to 94 nm thicknesses have SE $_A$  changing from 4 to 8 dB. Comparing these values with Fig. 2(b), we can estimate an absorption of 40%. The monolayer assembly deposition method reported by Yun et~al.  $^{29}$  demonstrates similar SE and sheet resistance values (i.e., sheet resistance of 233  $\Omega$ /sq for 7 nm film).

Measured S-parameters are used to calculate the sheet impedance of the film using Eq. (9). Results are displayed in Figs. S2(a) and S2(b). Sheet impedance does not exhibit frequency dependence; hence, averaged impedance values are plotted in Fig. 3(a). Sheet resistance decreases with thickness from 200 to  $20 \Omega/\text{sq}$  for 4 and 40 nm-thick films, respectively. For the 4 nm-thick film, the sheet resistance is close to half of the air-filled waveguide impedance  $Z_0$ , leading to 50% absorption. With increasing thickness, the absorption parameter slowly drops; however, even for 13 nm-thick film, with sheet resistance equal to  $100 \Omega/\text{sq}$ , the absorption is 44%. Films exhibit capacitive behavior, which is likely due to surface morphology and capacitance between the conductive film and the waveguide. This is supported by negative sheet reactance, which approaches zero with increasing thickness. Figure 3(b) correlates sheet resistance to absorbance and SE<sub>A</sub> SE<sub>A</sub> of the films, showing a good correlation with previously reported results. Sheet impedance values were backed up by sheet resistance at DC measured by the 4-point probe method. Sheet resistance at DC is measured over the effective area of the 4-point probe, and multiple measurements over the sample area were conducted for accurate estimation. The method requires physical contact of the probes with the sample, which might lead to damage to the surface and inaccurate results. Five measurements per sample were performed, from which the average and standard deviation were calculated. Standard deviation decreases with thickness from 20 to  $0.6\,\Omega/\text{sq}$ . Measurements were



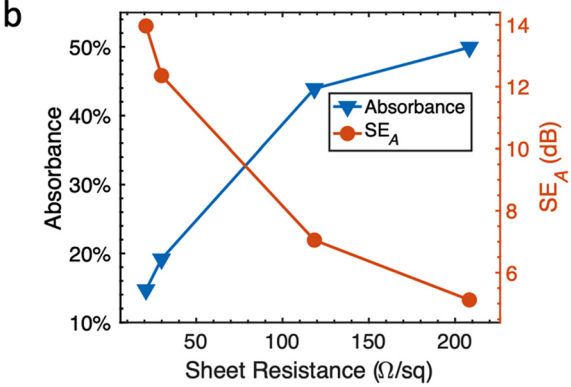


**FIG. 3.** (a) Sheet resistance (blue) decreases with thickness from 208 to 21  $\Omega/\text{sq}$ . DC values in red match microwave measurement. Sheet resistance plotted in yellow is due to the gap between the film and the flange of the waveguide. (b) Absorbance and SE<sub>A</sub> dependence on sheet resistance.

done on the central area of the film to avoid sheet resistance errors due to edge effects. The applied waveguide method, on the other hand, is contactless, and it analyzes the surface area equal to the cross section (22.4  $\times$  10.1 mm), being more sensitive to surface morphology. Sheet resistance is stable around the entire X-band frequency range. Waveguide measurements were averaged over 3201 data points. Error in RF measurements is strongly dependent on the transmission signal, and with its decrease, the overall analysis becomes erroneous.

To analyze the bulk in-plane conductivity, the film conductance value was plotted against thickness in Fig. 4. Results follow the linear behavior reported by Dillon  $et~al.;^{37}$  slight deviations are due to surface morphology. Conductivity values for DC are estimated to be 1.43  $\times$  10 $^6$  S/m, and for AC, it is  $1.20\times10^6$  S/m. The deviations between AC and DC sheet conductance values are within the errors of the measurements and are negligible when surface roughness is taken into account. This endorses the same mechanism of charge carrier transport occurring at DC to microwave range.  $^{38,39}$  Conductivity values for nanometer films are the same as those previously reported in the literature for micrometer films using the transmission line method.  $^{18,19}$ 

Since DC and AC conductivities are within the experimental error, the real part of conductivity can be interpreted as average. Assuming the real part of conductivity does not change with thickness, the application of the Drude model allows us to estimate relaxation

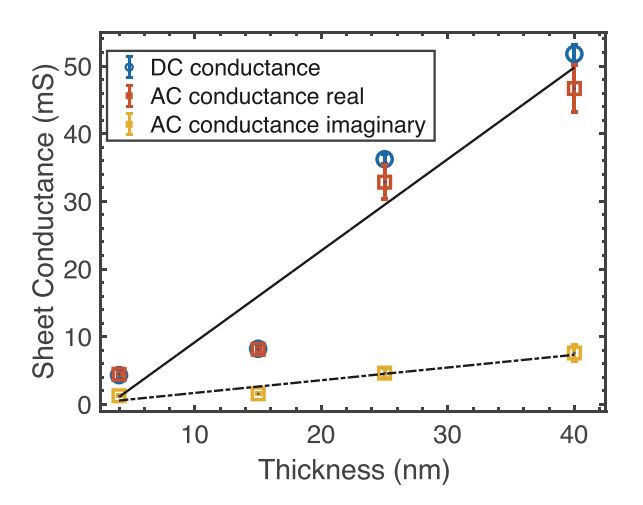


**FIG. 4.** Sheet conductance change with thickness follows a linear trend. Calculation of the slope allows us to estimate the real part of conductivity as 1.30  $\times$  10<sup>6</sup> S/m and the imaginary part as 1.9  $\times$  10<sup>5</sup> S/m.

times for  ${\rm Ti_3C_2T_x}$  spray-coated films  $\sigma=\sigma_{DC}/1-i\omega\tau$  ( $\omega$ —angular frequency and  $\tau$ —relaxation time). The calculated relaxation time is around 2.3 ps and is likely corresponding to the characteristic length scale  $L_\omega=\sqrt{D/\omega}$  (D—diffusion length of charge carrier) at GHz frequency range. This parameter correlates with the surface morphology, as flake boundaries contribute to an increase in resistance and higher surface roughness.

Results reported in this paper are in agreement with THz measurements done on monolayer assembled films.<sup>22</sup> Sheet resistance values at which maximum absorption occurs are relative to the free space impedance (188  $\Omega$  for free space and  $\sim$ 250  $\Omega$  for the waveguide). Despite measurements done at different frequency ranges, absorption maximum due to impedance matching occurs in the range of 4 nm for spray-coated films and 10.2 nm for monolayer assembly. DC sheet resistance values for spray-coated films vary from 250 to  $20 \Omega/\text{sq}$ , while monolayer assemblies give sheet resistance of  $10^3$ – $10^4 \Omega/\text{sq}$  for corresponding thicknesses of a few nanometers. The difference on the order of magnitude in DC values is due to the monolayer assembly deposition method, involving acetate that hinders conductivity by isolating flakes, creating a dielectric layer, and affecting the film thickness. In contrast, spray coating is done with water solvent most of which is removed during air drying. Close values of sheet conductance achieved through GHz and THz measurements allow us to conclude that both inter and intra-flake mechanisms participate in charge transfer from DC to THz. This allows us to hypothesize that the electron transport mechanism of MXene can be described as for ultrathin metal films (UTMF) when a percolation network is established. For example, Au films with thicknesses around 5 nm have been shown to meet the impedance matching condition when their conductivity is on the order 10<sup>6</sup> S/m and allows broadband absorption from microwave<sup>7,8</sup> to IR<sup>6,24</sup> frequency range.

In conclusion,  ${\rm Ti_3C_2T_x}$  film interaction with electromagnetic radiation from 8.2 to 12.4 GHz (X-band) was analyzed as a function of the film thickness. The films have shown high absorbance values up to 49% for 4 nm films. With increasing thickness, reflection becomes dominant. This is explained by sheet impedance matching half of the

free space impedance, which allows for maximum absorption. The real part of the impedance is used to calculate AC conductivity values. Values are in close agreement with DC sheet resistance measured with the 4-point probe. Bulk in-plane conductivity was estimated to vary slightly between the two measurements. Conductivity approximated as an average between AC and DC values reaches  $1.30 \times 10^6$  S/m. This demonstrates that the conductivity mechanism is the same for DC and AC as well as behavior at microwave frequencies, which can be described by the Drude model. Based on agreement with the measurements performed in the THz range, it is possible to hypothesize that the MXene conductivity mechanism does not change from DC to THz. The conventional method of reporting EMI SE is correlated with absolute values of transmitted, reflected, and absorbed power, which allows us to interpret previous results on MXene EMI shielding.

Based on these results, MXene films can be used as efficient absorbers in a wide frequency range when the impedance condition is matched. Conductivity is independent from frequency, leading to absorbance in the broad frequency range from RF to THz. Multiple few-nanometer-thin films can be assembled into heterostructures and metamaterials.  ${\rm Ti}_3{\rm C}_2{\rm T}_x$  performance is the same as for ultrathin Au films; however, the use of abundant elements (Ti, C, and O), ease of processibility, and singular and tunable physicochemical properties make MXenes appealing for future technologies.

See the supplementary material for figures demonstrating frequency dependence of absorbance, transmittance, and reflectance as well as AC impedance.

This work was supported by the U.S. National Science Foundation (No. ECCS-2034114). The authors thank Professor Aaron Fafarman for valuable discussions.

## AUTHOR DECLARATIONS Conflict of Interest

The authors have no conflicts to disclose.

## **Author Contributions**

Roman Rakhmanov: Conceptualization (lead); Data curation (lead); Formal analysis (lead); Investigation (lead); Methodology (lead); Visualization (lead); Writing – original draft (lead); Writing – review & editing (equal). Christopher Shuck: Data curation (equal); Formal analysis (equal); Writing – review & editing (equal). Jamal Al Hourani: Data curation (equal); Formal analysis (equal); Investigation (equal); Writing – review & editing (equal). Stefano Ippolito: Data curation (equal); Formal analysis (equal); Investigation (equal); Writing – review & editing (equal). Yury Gogotsi: Conceptualization (lead); Funding acquisition (lead); Supervision (lead); Writing – review & editing (equal). G. Friedman: Conceptualization (lead); Funding acquisition (lead); Supervision (lead); Writing – review & editing (equal).

## **DATA AVAILABILITY**

The data that support the findings of this study are available from the corresponding authors upon reasonable request.

#### **REFERENCES**

- <sup>1</sup>S. Dang, O. Amin, B. Shihada, and M.-S. Alouini, "What should 6G be?," Nat. Electron. 3(1), 20–29 (2020).
- <sup>2</sup>M. Médard, "Is 5 just what comes after 4?," Nat. Electron. 3(1), 2–4 (2020).
- <sup>3</sup>C. M. Watts, X. Liu, and W. J. Padilla, "Metamaterial electromagnetic wave absorbers," Adv. Mater. 24(23), OP98–OP120 (2012).
- <sup>4</sup>W. Woltersdorff, "Über die optischen Konstanten dünner Metallschichten im langwelligen Ultrarot," Z. Phys. **91**(3), 230–252 (1934).
- <sup>5</sup>A. E. Kaplan, "Metallic nanolayers: A sub-visible wonderland of optical properties," J. Opt. Soc. Am. B 35(6), 1328–1340 (2018).
- <sup>6</sup>N. Luhmann, D. Hùj, M. Piller, H. Kähler, M.-H. Chien, R. G. West, U. L. Andersen, and S. Schmid, "Ultrathin 2 nm gold as impedance-matched absorber for infrared light," Nat. Commun. 11(1), 2161 (2020).
- <sup>7</sup>M. Haddadi. M, B. Das, J. Jeong, S. Kim, and D.-S. Kim, "Near-maximum microwave absorption in a thin metal film at the pseudo-free-standing limit," Sci. Rep. 12(1), 18386 (2022).
- <sup>8</sup>S. Li, S. Anwar, W. Lu, Z. H. Hang, B. Hou, M. Shen, and C.-H. Wang, "Microwave absorptions of ultrathin conductive films and designs of frequency-independent ultrathin absorbers," AIP Adv. 4(1), 017130 (2014).
- <sup>9</sup>M. Walther, D. G. Cooke, C. Sherstan, M. Hajar, M. R. Freeman, and F. A. Hegmann, "Terahertz conductivity of thin gold films at the metal-insulator percolation transition," Phys. Rev. B 76(12), 125408 (2007).
   <sup>10</sup>A. Thoman, A. Kern, H. Helm, and M. Walther, "Nanostructured gold films as
- <sup>10</sup> A. Thoman, A. Kern, H. Helm, and M. Walther, "Nanostructured gold films as broadband terahertz antireflection coatings," Phys. Rev. B 77(19), 195405 (2008).
- <sup>11</sup>M. Naguib, M. Kurtoglu, V. Presser, J. Lu, J. Niu, M. Heon, L. Hultman, Y. Gogotsi, and M. W. Barsoum, "Two-dimensional nanocrystals produced by exfoliation of Ti<sub>3</sub>C<sub>2</sub>T<sub>x</sub>," Adv. Mater. 23(37), 4248–4253 (2011).
- <sup>12</sup>G. Deysher, C. E. Shuck, K. Hantanasirisakul, N. C. Frey, A. C. Foucher, K. Maleski, A. Sarycheva, V. B. Shenoy, E. A. Stach, B. Anasori, and Y. Gogotsi, "Synthesis of Mo<sub>4</sub>VAlC<sub>4</sub> phase and two-dimensional Mo<sub>4</sub>VC<sub>4</sub> MXene with five atomic layers of transition metals," ACS Nano 14(1), 204–217 (2020).
- <sup>18</sup>M. Downes, C. E. Shuck, R. W. Lord, M. Anayee, M. Shekhirev, R. J. Wang, T. Hryhorchuk, M. Dahlqvist, J. Rosen, and Y. Gogotsi, "M<sub>5</sub>X<sub>4</sub>: A Family of MXenes," ACS Nano 17(17), 17158–17168 (2023).
- 14. A. VahidMohammadi, J. Rosen, and Y. Gogotsi, "The world of two-dimensional carbides and nitrides (MXenes)," Science 372(6547), eabf1581 (2021).
- <sup>15</sup>M. Han, C. E. Shuck, R. Rakhmanov, D. Parchment, B. Anasori, C. M. Koo, G. Friedman, and Y. Gogotsi, "Beyond Ti<sub>3</sub>C<sub>2</sub>T<sub>x</sub>: MXenes for electromagnetic interference shielding," ACS Nano 14(4), 5008–5016 (2020).
- <sup>16</sup>A. Iqbal, P. Sambyal, and C. M. Koo, "2D MXenes for electromagnetic shielding: A review," Adv. Funct. Mater. 30(47), 2000883 (2020).
- 17 A. Sarycheva, A. Polemi, Y. Liu, K. Dandekar, B. Anasori, and Y. Gogotsi, "2D titanium carbide (MXene) for wireless communication," Sci. Adv. 4(9), eaau0920 (2018).
- $^{18}$  K. AlHassoon, M. Han, Y. Malallah, V. Ananthakrishnan, R. Rakhmanov, W. Reil, Y. Gogotsi, and A. S. Daryoush, "Conductivity extraction of thin  $\rm Ti_3C_2T_x$  MXene films over 1–10 GHz using capacitively coupled test-fixture," Appl. Phys. Lett. 116(18), 184101 (2020).
- <sup>19</sup>M. Han, Y. Liu, R. Rakhmanov, C. Israel, M. A. S. Tajin, G. Friedman, V. Volman, A. Hoorfar, K. R. Dandekar, and Y. Gogotsi, "Solution-processed Ti<sub>3</sub>C<sub>2</sub>T<sub>x</sub> MXene antennas for radio-frequency communication," Adv. Mater. 33(1), 2003225 (2021).
- <sup>20</sup> M. Han, C. E. Shuck, A. Singh, Y. Yang, A. C. Foucher, A. Goad, B. McBride, S. J. May, V. B. Shenoy, E. A. Stach, and Y. Gogotsi, "Efficient microwave absorption with V<sub>n+1</sub>C<sub>n</sub>T<sub>x</sub> MXenes," Cell Rep. Phys. Sci. 3(10), 101073 (2022).

- <sup>21</sup>G. Li, K. Kushnir, Y. Dong, S. Chertopalov, A. M. Rao, V. N. Mochalin, R. Podila, and L. V. Titova, "Equilibrium and non-equilibrium free carrier dynamics in 2D Ti<sub>3</sub>C<sub>2</sub>T<sub>x</sub> MXenes: THz spectroscopy study," 2D Mater. 5(3), 035043 (2018).
- <sup>22</sup>T. Zhao, P. Xie, H. Wan, T. Ding, M. Liu, J. Xie, E. Li, X. Chen, T. Wang, Q. Zhang, Y. Wei, Y. Gong, Q. Wen, M. Hu, C.-W. Qiu, and X. Xiao, "Ultrathin MXene assemblies approach the intrinsic absorption limit in the 0.5–10 THz band," Nat. Photonics 17(7), 622–628 (2023).
- <sup>23</sup>G. Li, N. Amer, H. A. Hafez, S. Huang, D. Turchinovich, V. N. Mochalin, F. A. Hegmann, and L. V. Titova, "Dynamical control over terahertz electromagnetic interference shielding with 2D Ti<sub>3</sub>C<sub>2</sub>T<sub>y</sub> MXene by ultrafast optical pulses," Nano Lett. 20(1), 636–643 (2020).
- <sup>24</sup>D. Martínez-Cercós, B. Paulillo, R. A. Maniyara, A. Rezikyan, I. Bhattacharyya, P. Mazumder, and V. Pruneri, "Ultrathin metals on a transparent seed and application to infrared reflectors," ACS Appl. Mater. Interfaces 13(39), 46990–46997 (2021).
- 25 J. Krupka, "Frequency domain complex permittivity measurements at microwave frequencies," Meas. Sci. Technol. 17(6), R55–R70 (2006).
- 26F. Costa, "Surface impedance measurement of resistive coatings at microwave frequencies," IEEE Trans. Instrum. Meas. 62(2), 432–437 (2013).
- 27R. J. Collier and D. G. Hasko, "Measurement of the sheet resistance of resistive films on thin substrates from 120 to 175 GHz using dielectric waveguides," J. Appl. Phys. 91(4), 2547–2549 (2002).
- <sup>28</sup>X.-C. Wang, A. Díaz-Rubio, and S. A. Tretyakov, "An accurate method for measuring the sheet impedance of thin conductive films at microwave and millimeter-wave frequencies," IEEE Trans. Microwave Theory Tech. 65(12), 5009–5018 (2017).
- <sup>29</sup>T. Yun, H. Kim, A. Iqbal, Y. S. Cho, G. S. Lee, M.-K. Kim, S. J. Kim, D. Kim, Y. Gogotsi, S. O. Kim, and C. M. Koo, "Electromagnetic shielding of monolayer MXene assemblies," Adv. Mater. 32(9), 1906769 (2020).
- 30 L. D. Landau, E. M. Lifshitz, and A. L. King, "Electrodynamics of continuous media," Am. J. Phys. 29(9), 647–648 (1961).
- <sup>31</sup>D. Reitz, "A review of: 'Electrodynamics of solids: Optical properties of electrons in matter,' "Mater. Manuf. Processes 20(6), 1005–1005 (2005).
- <sup>32</sup>J. C.-E. Sten and P. Koivisto, "Optimum transparent absorbers of electromagnetic waves," IEEE Trans. Electromagn. Compat. 50(4), 1011–1014 (2008).
- 33 M. Peng and F. Qin, "Clarification of basic concepts for electromagnetic interference shielding effectiveness," J. Appl. Phys. 130(22), 225108 (2021).
- <sup>34</sup>U. Hwang, J. Kim, M. Seol, B. Lee, I.-K. Park, J. Suhr, and J.-D. Nam, "Quantitative interpretation of electromagnetic interference shielding efficiency: Is it really a wave absorber or a reflector?," ACS Omega 7(5), 4135–4139 (2022).
- <sup>35</sup>D. M. Pozar, *Microwave Engineering*, 4th ed. (Wiley Global Education, 2011).
   <sup>36</sup>T. S. Mathis, K. Maleski, A. Goad, A. Sarycheva, M. Anayee, A. C. Foucher, K. Hantanasirisakul, C. E. Shuck, E. A. Stach, and Y. Gogotsi, "Modified MAX
- phase synthesis for environmentally stable and highly conductive Ti<sub>3</sub>C<sub>2</sub> MXene," ACS Nano 15(4), 6420–6429 (2021).

  37A. D. Dillon, M. J. Ghidiu, A. L. Krick, J. Griggs, S. J. May, Y. Gogotsi, M. W.
- A. D. Dillon, M. J. Ghidiu, A. L. Krick, J. Griggs, S. J. May, Y. Gogotsi, M. W. Barsoum, and A. T. Fafarman, "Highly conductive optical quality solution-processed films of 2D titanium carbide," Adv. Funct. Mater. 26(23), 4162–4168 (2016).
- <sup>38</sup>J. L. Hart, K. Hantanasirisakul, A. C. Lang, B. Anasori, D. Pinto, Y. Pivak, J. T. van Omme, S. J. May, Y. Gogotsi, and M. L. Taheri, "Control of MXenes' electronic properties through termination and intercalation," Nat. Commun. 10(1), 522 (2019).
- <sup>39</sup>W. Zheng, B. Sun, D. Li, S. M. Gali, H. Zhang, S. Fu, L. Di Virgilio, Z. Li, S. Yang, S. Zhou, D. Beljonne, M. Yu, X. Feng, H. I. Wang, and M. Bonn, "Band transport by large Fröhlich polarons in MXenes," Nat. Phys. 18(5), 544–550 (2022).